International Journal of Biological Macromolecules 306 (2025) 141755

Contents lists available at ScienceDirect

International Journal of Biological Macromolecules

journal homepage: www.elsevier.com/locate/ijbiomac

Exploring acid hydrolysis conditions and extended mechanical processing for producing cellulose nanocrystal and nanofibrils from pineapple leaf fibers

Fernanda Andrade Tigre da Costa [a,b,*], Alain Dufresne [b], Tao Song [c], Duclerc Fernandes Parra [a]

[a] Nuclear and Energy Research Institute, IPEN–CNEN/SP, Av. Prof. Lineu Prestes, 2242 – Cidade Universitária, CEP 05508-000, São Paulo, SP, Brazil
[b] University Grenoble Alpes, CNRS, Grenoble INP, LGP2, F-38000, Grenoble, France
[c] State Key Laboratory of Pulp and Paper Engineering, South China University of Technology, Guangzhou 510640, PR China

ARTICLE INFO

Keywords:
Pineapple leaf fiber (PALF)
Cellulose nanocrystals (CNC)
Cellulose nanofibrils (CNF)

ABSTRACT

This study investigates the potential of pineapple leaf fiber (PALF), as a renewable source, to produce cellulose nanofibrils (CNF) and cellulose nanocrystals (CNC), addressing a gap in the literature regarding optimal conditions for CNC extraction from PALF. Chemical analysis revealed a high α-cellulose content (78.14 %), making PALF suitable for nanocellulose production. MorFi analysis confirmed successful CNF production. Various hydrolysis conditions were explored to obtain CNC and some of them showed promising results. Characterization using FTIR, XRD, AFM, and TGA confirmed successful nanocellulose production. The CNCs exhibited a crystallinity index of 78.5 % and nanoscale dimensions (647–1105 nm, depending on the process), while CNF showed lengths of approximately 256 nm. TGA demonstrated that CNCs had lower thermal stability compared to cellulose and CNF due to reduced molecular weight and sulfate groups. CNC1 and CNC2, produced under optimized conditions (55 % acid concentration, 45 °C, 30 min), demonstrated superior properties, including high crystallinity and desirable nano-dimensions. This study highlights the novelty of using PALF for CNC production with tailored characteristics, paving the way for its application in biocomposites, drug delivery, and tissue engineering. PALF's availability and favorable composition make it a promising candidate for sustainable nanocellulose materials.

1. Introduction

The increasing demand for sustainable and high-performance materials has stimulated significant research towards the development of bio-based alternatives. Cellulose nanocrystals (CNC) and cellulose nanofibrils (CNF) have emerged as promising candidates due to their unique combination of properties. These nanomaterials boast high mechanical properties, low density, biocompatibility, renewability, and biodegradability, making them attractive for various applications including biocomposites, barrier films, sensors, and drug delivery systems [1,2].

Cellulose nanocrystals are typically rod-like nanocrystals extracted from the crystalline regions of cellulose, possessing exceptional mechanical strength and high aspect ratio [3]. Cellulose nanocrystals are needle-shaped (extended rods with tapered ends), rigid particles with a crystallinity of approximately 70 % [4]. Conversely, cellulose nanofibrils are elongated, high-surface-area flexible nanofibrils obtained through mechanical processing usually after chemical treatments [5]. Due to the high surface reactivity of nanocelluloses, they are often modified or combined with other compounds to obtain synergistic properties that can meet the requirements for certain applications [6].

Pineapple leaf fibers (PALF) represent a readily available and renewable source of cellulose with several advantages. PALF cultivation requires minimal resources and generates significant agricultural waste, offering a sustainable feedstock for biomaterial production [7]. Additionally, PALF exhibits high cellulose content and good mechanical properties, making it a promising candidate for CNC and CNF extraction [8]. Brazil, as the world's 4th largest producer of pineapples (2.32 million tons in 2021), after Costa Rica (2.94 million tons), Indonesia (2.89 million tons), and the Philippines (2.86 million tons), has a

* Corresponding author at: Department of chemistry and environment in Nuclear and Energy Research Institute, IPEN–CNEN/SP, Av. Prof. Lineu Prestes, 2242 - Butantã, São Paulo, SP 05508-000, Brazil.
E-mail address: fernanda.tigre@outlook.com (F.A.T. da Costa).

https://doi.org/10.1016/j.ijbiomac.2025.141755
Received 9 September 2024; Received in revised form 22 January 2025; Accepted 3 March 2025
Available online 4 March 2025

substantial potential to contribute to the development of cellulose-based products from pineapple leaves [9]. Pineapple leaves grow rapidly, which takes up almost 13–15 months to grow [10], providing a continuous supply of raw material. However, due to their fibrous nature and the limited commercial applications for the entire leaf, a significant portion is often discarded as waste. Estimates suggest that about 80 % of pineapple parts, including the crown, peels, leaves, core and stems, are discarded during pineapple harvesting, transportation and storage [11]. This waste is frequently burned, dumped, or left to decompose, presenting a significant opportunity for sustainable resource utilization [12].

Despite the promising potential of CNC and CNF derived from PALF, optimizing their production methods and the optimal conditions remain crucial. For instance, the extraction process significantly influences the final properties of these nanomaterials. Acid hydrolysis is a widely employed technique for CNC production, but harsh conditions can lead to cellulose degradation. Conversely, milder conditions may result in incomplete extraction [13]. This process selectively targets the amorphous regions of cellulose, breaking the glycosidic bonds while preserving the highly ordered crystalline segments [14]. Sulfuric acid hydrolysis is the primary method for industrial CNC production due to its effectiveness in isolating crystalline regions and imparting colloidal stability through sulfate half-ester groups [15,16].

Based on previous studies, the acid hydrolysis conditions for extracting cellulose nanocrystals from pineapple fiber can vary significantly. Dufresne [17] reported the use of 64 wt% sulfuric acid solution for 5 to 60 min at 45 °C with a 20 mL/g cellulose/solution ratio for pineapple leaf fiber. Anwar et al [18] optimized conditions for cellulose nanocrystals from bacterial cellulose produced from pineapple peel waste, achieving optimal results with 50 wt% of sulfuric acid solution, 25 to 40 min of hydrolysis time, and at a temperature of 50 °C. Prado & Spinacé [19] extracted CNC from pineapple crown leaf using 60 wt% of sulfuric acid solution for 1 h at 45 °C.

While other acids can be used, sulfuric acid's ability to introduce sulfate groups offers superior water dispersion and makes it the preferred choice for commercial applications [20]. There are various methods to produce CNC, with acid hydrolysis, ionic liquids, deep eutectic solvents, and enzymatic hydrolysis being considered more sustainable options. Alternative, less conventional methods include subcritical water, oxidation, and metal complexes [21]. In the case of CNF, they are commonly produced through three conventional methods: homogenization, grinding, and refining [22]. Similarly, mechanical processing parameters for CNF production require careful optimization to achieve the desired level of nanofibrillation while maintaining appropriate fiber length and crystallinity [23].

Given the variations in optimal conditions for PALF in the literature, this study aims to investigate a specific range of conditions to optimize CNC extraction from pineapple leaf fiber. This study delves into the production of CNC and CNF from PALF using an integrated processing combine with various techniques, included alkalization and bleaching procedures for extraction and sulfuric acid hydrolysis for CNC isolation. The influence of processing parameters on the final properties of these nanomaterials was investigated, focusing on optimizing the extraction process while preserving the inherent advantages of PALF. Through chemical analysis, x-ray diffraction (XRD), atomic force microscopy (AFM) and thermogravimetric analysis (TGA), we identified the most suitable conditions for producing high-quality CNC and CNF matching the requirements for various downstream applications.

2. Materials and methods

2.1. Materials

Pineapple leaves (*Ananas comosus* L. Merril) of the *Pérola* variety were collected from a plantation located in the city of Itatiba (Sao Paulo, Brazil). The reagents used for chemical treatments and characterizations of pineapple leaves were sodium hydroxide (NaOH) (purchased from Synth), glacial acetic acid (purchased from Control Lab LTDA), sodium chlorite ($NaClO_2$) 80 % (purchased from Petra Quimica), sulfuric acid 95–97 % (purchased from Merck), acetone (purchased from CA.AL).

2.2. Methods

2.2.1. Fiber extraction

For the extraction of pineapple leaf fibers (PALF), the leaves were separated and cut into pieces 1.5 to 2.5 cm long. After being washed to remove impurities, such as remnants of soil from the plantation, the leaves were added to a drying oven (Tecnomeca, Brazil) with air circulation for 72 h at 65 °C. The dried leaves were crushed in a Willye mill TE-650 from Tecnal. And then, the PALF was sieved on a 16 TY mesh particle size analysis sieve, equivalent to 1 mm.

2.2.2. Extraction of cellulose

The extraction of cellulose from PALF was carried out as frequently described in the literature [24,25] by alkaline and bleaching procedures to remove hemicelluloses and lignin. Initially, PALF was treated with a 0.2 N NaOH solution for 90 min at 100 °C under mechanical stirring using a propeller stirrer (RW 24, IKA-WERK, Germany) with a speed of 100 rpm, in which the ratio of PALF to alkaline solution was 1:10. After rinsing with water to remove the liquid containing dissolved hemicelluloses, lignin and other extractives, the fibers extracted through alkaline treatment were bleached in a solution of 7 wt% sodium chlorite and 1.4 wt% acetic acid under continuous stirring at 80 °C for 4 h. The fiber/solution ratio was 1:16. After bleaching, the fibers were washed several times with water to remove the residual chemicals and then dried in an oven at 65 °C for 72 h.

2.2.3. Extraction of cellulose nanofibrils (CNF)

Cellulose nanofibrils were obtained through mechanical action by ball milling. Grinding was carried out in a tumbler ball mill, model Q298–1 from Quimis Aparelhos Científicos, with an alumina ceramic flask with a capacity of 2.5 L and alumina grinding balls with three different diameters (18 balls of 10 mm, 8 balls of 19 mm and 5 balls of 50 mm) at a speed of 150 rpm for an extended period of 196 h to ensure the production of nanoparticles.

2.2.4. Extraction of cellulose nanocrystals (CNC)

CNC was prepared by acid hydrolysis treatment using sulfuric acid under different conditions, as shown in Table 1. These conditions were selected based on previous studies [17–19] on similar fiber sources, such as pineapple leaf, peel, and crown leaf. Considering the variability reported in the literature, this study aims to investigate and optimize the conditions for cellulose nanocrystal extraction from PALF. While a 64 wt % sulfuric acid concentration has been reported for pineapple leaf fiber, our preliminary experiments indicated significant degradation under these conditions. Therefore, to optimize the process, we explored lower acid concentration (55 %) and adjusted reaction time and cellulose concentration to achieve optimal CNC quality. Immediately after

Table 1
Denomination of CNC samples according to the method of obtaining.

Nomenclature	Acid Concentration (%wt of H_2SO_4 in H_2O)	Temperature of hydrolysis (°C)	Time of hydrolysis (min)	Sample-solution ratio (mg/mL)
CNC1	55	45	30	20
CNC2	55	45	30	125
CNC3	55	45	60	50
CNC4	64	45	15	50
CNC5	64	45	30	20
CNC6	64	55	30	25
CNC7	64	55	60	25

hydrolysis, the suspension was diluted ten times with cold distilled water to stop the reaction. The suspension was then transferred to centrifuge bottles and centrifuged at 10,000 rpm for 10 min, this process was repeated twice. The samples were then dialyzed against distilled water to remove excess acid for a period of 1 week until the pH reached the pH near to the one of water. The resulting CNC suspension was sonicated in a water bath for 2 min. The overall process for producing CNF and CNC from pineapple leaf fiber is illustrated in Fig. 1. The CNC yield was determined by drying a known volume of the CNC suspension at 105 °C for 12 h in an air-circulating oven.

2.3. Characterizations

2.3.1. Chemical composition of PALF

The chemical composition of the *PALF* was determined as follows: the amount of extractives in the fiber was determined according to TAPPI T204 cm-97 [26] standard method using acetone as reagent in a Soxhlet apparatus for 4.2 h which consisted of 24 repetition cycles. The moisture content of the PALF was measured according to the TAPPI T264 cm-07 [27] standard. Ash content was determined by standard method of TAPPI T211 om-02 [28] standard method. The acid-insoluble lignin content was determined according to TAPPI T222 om-02 [29] standard method using sulfuric acid solution at 72 % (24 N) as reagent. The percentage of holocellulose was calculated according to the Wise and Murphy method [30] in which the extractive-free fibers were boiled in a mixture of $NaClO_2$ and acetic acid (2.5 g and 1 mL, respectively, for 120 mL of water) for 5 h at 70 °C and after the first and second hour, the same amounts of the mixture were added. The determination of the alpha, beta and gamma cellulose content was carried out according to the TAPPI T203 cm-99 [31] standard method. Cellulose content was considered as the portion of holocellulose that consisted of alpha-cellulose, while hemicellulose was considered as the remaining difference between holocellulose and alpha-cellulose.

2.3.2. Morphological analysis of fibrous suspensions (MorFi)

Size distribution and fine content of cellulose and CNF were determined by MorFi analysis. Tests were performed twice in a MorFi fiber analyzer (NEO LB-01, Techpap, France). Fibers were suspended at 25 mg/L in water and shaken with ultra turrax (T25 EC D S000, IKA, Germany) at 8000 rpm for 3 min. The fiber/fine limit was set at 50 μm in length, and the number of analyzed fibers was set at 20,000. Following this, the fine content, fiber content, and mean area-weighted length were determined.

2.3.3. Fourier transform infrared spectroscopy (FTIR)

FTIR was carried out to identify the type of bonds and components present in the fibers. The spectra were recorded using Perkin Elmer/Spectrum 65 in 4000 to 400 cm^{-1} range at resolution of 4 cm^{-1} with 16 accumulations. The powdered fibers were mixed with KBr in a ratio of 1:99 to pressed into discs.

2.3.4. X-ray diffraction (XRD)

The crystallinity of PALF, cellulose and CNF was studied using an X-ray diffractometer X'Pert Pro MPD from the PANalytical company, equipped with CuKα radiation (λ = 1.5418 Å) in the 2θ range 6–60°. The experiments were performed in the reflection mode with the Bragg-

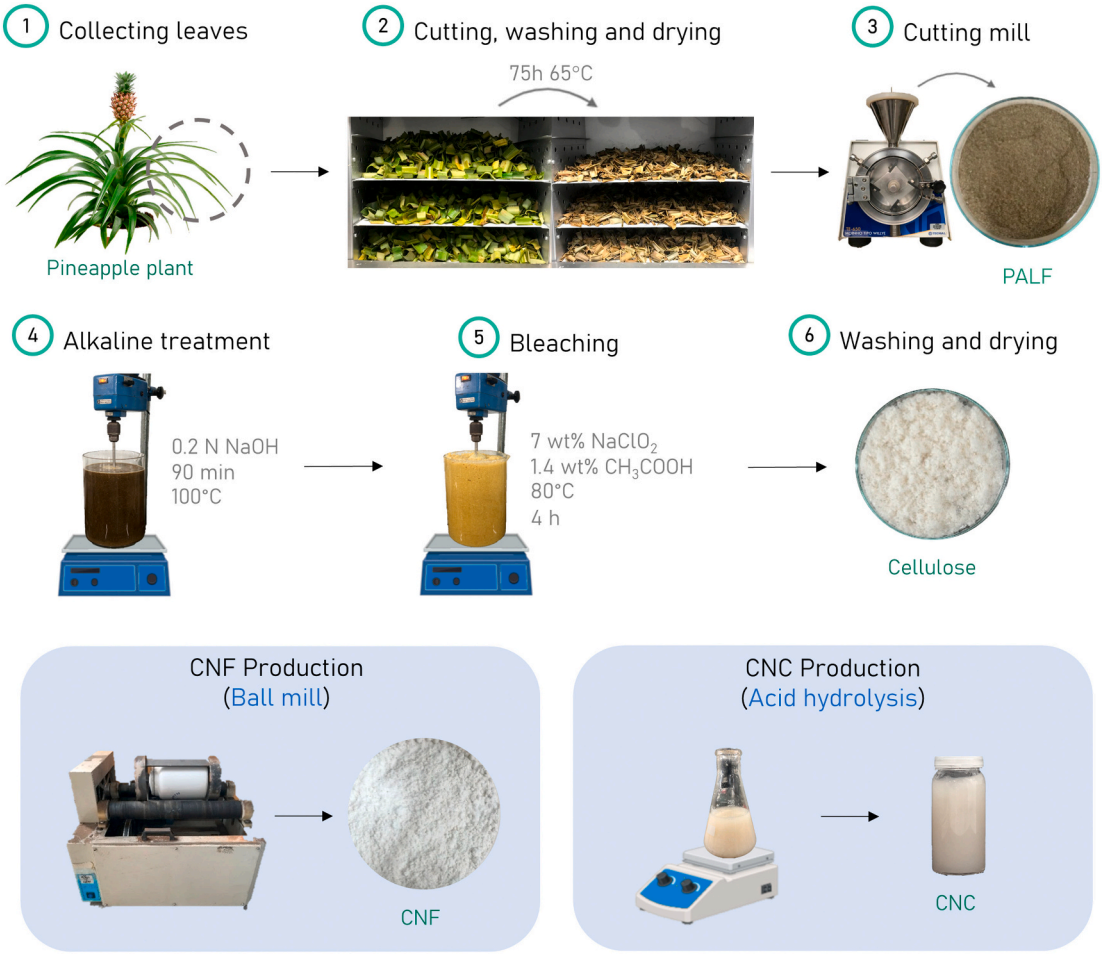

Fig. 1. General scheme of CNF and CNC production from PALF.

Brentano geometry at a scan speed of 1°/min. The crystallinity index (CrI) of the samples was calculated according to the Segal empirical method shown in Eq. 1 [32].

$$CrI = \frac{I_t - I_a}{I_t} \times 100 \quad (1)$$

Where I_t is the total intensity of the (200) peak for cellulose I_β at 22.7° 2θ and I_a is the amorphous intensity at 18° 2θ for cellulose I_β.

2.3.5. Atomic force microscopy (AFM)

Atomic force microscopy was used to observe the morphology of the CNC and CNF obtained after the various treatments. Measurements were performed on a Multimodal AFM (Dimension Icon, Veeco/Bruker, Germany) in a tapping mode. The samples were observed after adding a drop of 0.02 wt% CNC and CNF suspension onto a mica substrate and being dried at room temperature. AFM images were analyzed using NanoScope Analysis software version 1.40, to determine the dimensions of the fibers.

2.3.6. Thermogravimetric analysis (TGA)

The thermal decomposition behavior of the cellulose samples was investigated using thermogravimetric analysis (TGA) conducted on a Mettler Toledo TGA/DSC 3+ STARe System (Mettler Toledo, Greifensee, Switzerland). For each experiment, 10 ± 3 mg of the sample was weighed into a 70 μL alumina crucible without a lid. The heating program employed a constant rate of 10 °C/min in the temperature range from 30 °C to 600 °C with a nitrogen flow at a rate of 50 mL/min to maintain an inert atmosphere.

3. Results and discussion

3.1. Chemical composition determination of PALF

The chemical composition of the fiber extracted from the pineapple leaf of the Pérola variety is reported in Table 2. PALF exhibits a unique chemical composition characterized by a significant proportion of holocellulose (64.67 %), highlighting its potential as a source of cellulosic materials. Holocellulose encompasses both cellulose and hemicellulose, which can be further differentiated based on their solubility in various chemical solutions [33]. Delving deeper into the holocellulose fraction, the analysis reveals a noteworthy content of α-cellulose (78.14 %), the most crystalline and desirable form of cellulose due to its superior mechanical strength and thermal stability [34]. This high α-cellulose content suggests promising applications for PALF in the development of strong and durable biocomposites. However, the presence of β-cellulose (8.11 %) and γ-cellulose (13.75 %) indicates the existence of less ordered and more amorphous cellulose fractions within the fiber. These cellulose fractions are generally less desirable for certain applications due to their lower mechanical properties. Nonetheless, the total cellulose content (α-cellulose) of PALF is up to 50.53 %, highlighting its potential as a valuable source of cellulosic material.

Beyond cellulose, PALF also contains a moderate amount of hemicellulose (14.14 %). Hemicellulose is a polysaccharide with a more branched and amorphous structure compared to cellulose [35]. While hemicellulose can potentially offer some functional benefits in biocomposites, its presence has positive correlation with moisture sorption and biodegradation [36]. The analysis further reveals the presence of lignin (18.95 %) within the fiber. Lignin is a complex aromatic biopolymer that acts as a natural binder between cellulose and hemicellulose, providing rigidity and structural support to the plant cell wall [35]. However, high lignin content can hinder the accessibility of cellulose for processing and ultimately reduce the mechanical properties of biocomposites [37]. Therefore, optimizing the lignin removal process during fiber treatment may be necessary for certain applications.

Finally, the presence of extractives (4.14 %), ash (6.78 %), and moisture (2.27 %) contributes to the overall composition of PALF. Extractives are low molecular weight components that can influence various fiber properties, while ash represents the inorganic residue remaining after combustion. Moisture content is an important factor for storage and processing considerations. Therefore, the chemical composition of PALF, characterized by a high holocellulose content with a significant portion of desirable α-cellulose, presents promising potential for various applications. However, the presence of lignin and less ordered cellulose fractions alongside hemicellulose necessitates careful consideration during processing and material development to maximize the utilization of PALF as a valuable source of cellulosic biomaterial.

Table 2
Chemical composition of the pineapple leaf fiber.

Component	PALF composition (%)
Holocellulose	64.67 ± 2.29
α-cellulose	78.14 ± 0.35
β-cellulose	8.11 ± 0.51
γ-cellulose	13.75 ± 0.37
Cellulose	50.53 ± 1.80
Hemicellulose	14.14 ± 0.64
Lignin	18.95 ± 0.19
Extractives	4.14 ± 0.92
Ash	6.78 ± 0.08
Moisture	2.27 ± 0.03

3.2. MorFi analysis

MorFi analysis was employed to comprehensively characterize the size distribution and fine content of both cellulose from PALF and resulted CNF. In this study, particles with a length less than 50 μm were classified as fines, while those exceeding 50 μm were categorized as fibers. Table 3 summarizes the findings, revealing a significant contrast between the size distributions of the two materials. As anticipated, cellulose exhibited a predominance of fibers, constituting approximately 90 % of the sample by area. These fibers possessed an average length of 528 μm, highlighting their coarse nature. Conversely, CNF displayed a dramatic shift towards the fine fraction. Notably, 85 % of the CNF sample fell below the 50 μm threshold, signifying a successful conversion process that yielded a population of nanofibrils. However, a minor fraction (15 %) of the CNF material remained as fibers, with an average length of 116 μm. These residual fibers likely represent incompletely fibrillated cellulose fragments that were not fully converted during the CNF production process.

Fig. 2 presents the data for CNF in detail, including the percentage of fines and fibers categorized by three criteria: area of the observed frame, length, and length-weighted length. The analysis revealed a significant enrichment of fines within the CNF population. When measured by area, over 85 % of the CNF material fell below the 50 μm threshold. This dominance of fines was further amplified when considering length and length-weighted length, with both metrics exceeding 97 % for fibers smaller than 50 μm. Interestingly, the data also highlights a clear distinction in average fiber length based on size. Fibers exceeding 50 μm possessed a considerably longer average length of 107 μm compared to their smaller counterparts, which averaged only 19 μm in length. These findings offer valuable insights into the dimensional characteristics of the CNF material, suggesting a population enriched with shorter and finer fibers.

Table 3
MorFi analysis of cellulose and CNF suspensions.

Sample	Fiber content (millions/g of pulp)	Fine content (% in area)	Mean area-weighted length of the fibers (μm)
Cellulose	34.10 ± 2.65	10.1 ± 0.4	528.0 ± 8.5
CNF	11.69 ± 0.02	85.5 ± 0.5	116.0 ± 4.2

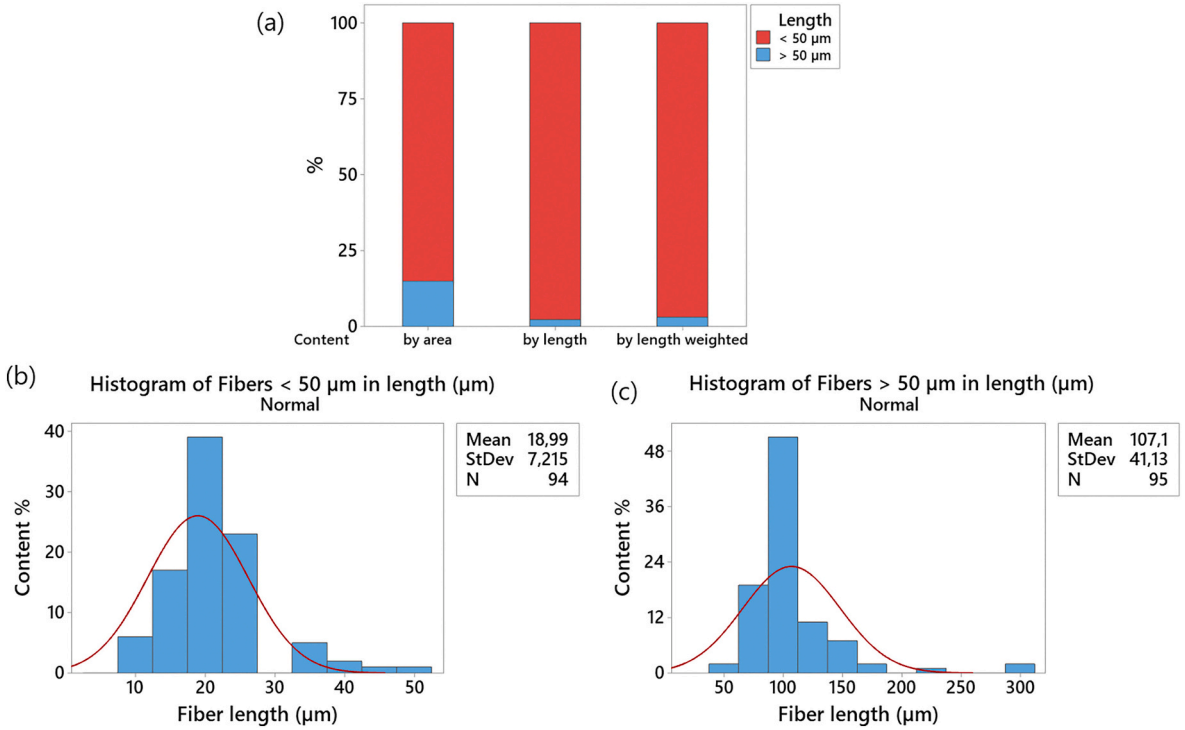

Fig. 2. MorFi analysis of CNF suspensions obtained: (a) proportion of fibers in the solution larger and smaller than 50 µm calculated by 3 different methods; (b) distribution of fibers smaller than 50 µm; (c) distribution of fibers larger than 50 µm.

3.3. CNC production

The investigation into the seven different conditions for obtaining CNC depicted in Fig. 3 revealed some interesting findings. Notably, the combination of 64 % acid concentration and 55 °C temperature resulted in a concerningly rapid degradation effect on the utilized PALF cellulose (CNC6 and CNC7 samples). This is likely due to the aggressive nature of the concentrated acid at elevated temperature, breaking down the cellulose structure. By reducing the temperature to 45 °C, visually better results were obtained. CNC5, for instance, prepared at 45 °C, exhibited a rapid darkening with increased hydrolysis time during the reaction (Fig. S1). However, this darkening effect appeared to be solely a characteristic of the pre-centrifugation stage. The final CNC sample, after centrifugation, displayed no darkening, suggesting that the observed color change might be attributed to impurities or byproducts separating out during the hydrolysis process. This observation further strengthens the notion that at 64 % acid concentration, even a seemingly minor temperature increases from 45 °C to 55 °C can induce significant

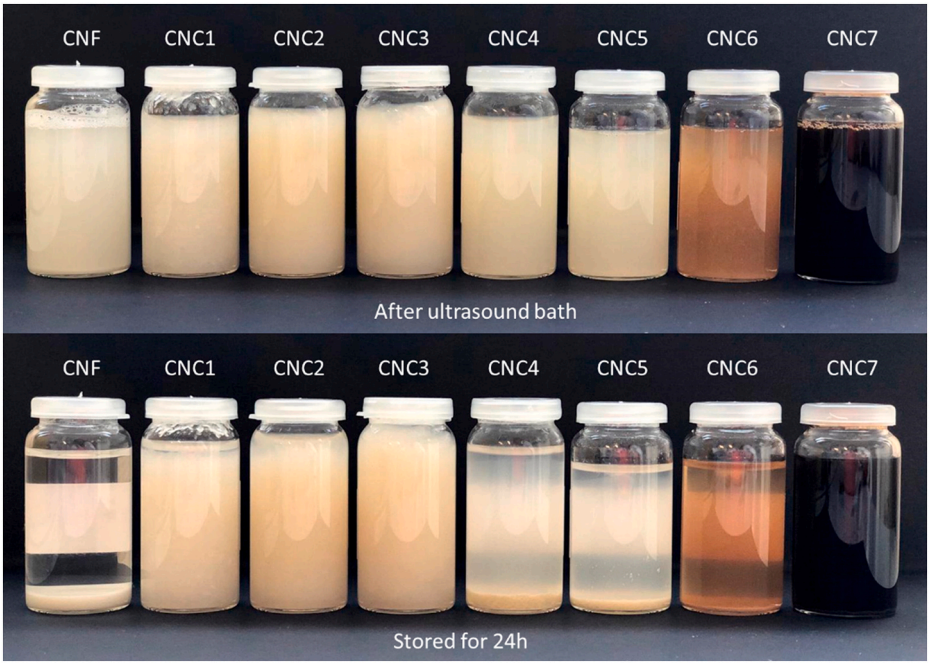

Fig. 3. Photographs of CNF and CNC suspensions after ultrasound bath and storage for 24 h.

degradation of PALF cellulose.

The precipitation of CNF suspension was possibly due to the extensive ball milling process, which has reduced the fibers to aggregated particles lacking fibrillation, resulting in poor dispersion stability and subsequent precipitation [38,39]. The observed precipitation of CNC samples (CNC4 to CNC7) prepared with high sulfuric acid concentrations (64 %) after 24 h is likely due to increased surface charge from sulfate groups introduced during hydrolysis. These negatively charged groups enhance electrostatic repulsion, stabilizing the CNC suspension. However, over time, factors such as ionic strength, pH changes, or insufficient surface charge can reduce this repulsion, leading to aggregation and precipitation [40].

Table 4 presents the yield percentages of CNCs obtained under different hydrolysis conditions. These values are consistent with previous literature findings [16,17,41,42]. The high yield of CNC1 is likely attributed to the presence of some microfibers in the sample. This is supported by Fig. 3, which shows evidence of sedimentation in CNC1 after 24 h. It is observed that increasing the hydrolysis time and sample-to-solution ratio led to a decrease in yield (CNC2 and CNC3 samples). As reported by Dufresne [17], increasing hydrolysis temperature or time can negatively impact the yield of cellulose nanocrystals. Similarly, increasing the sulfuric acid concentration from 55 % to 64 % resulted in a significant yield reduction (CNC4 to CNC7). It is known that using a slightly lower sulfuric acid concentration (58 %) compared to the standard 64 % can minimize cellulose loss to sugars, leading to improved nanocrystal yield [16]. Additionally, it has been reported for bleached kraft eucalyptus pulp that the nanocrystal yield is influenced by two primary processes: cellulose depolymerization at acid concentrations below 58 % and nanocrystal degradation at concentrations above 64 % [42].

Different hydrolysis times and solution-to-sample concentration ratios were employed to strike a balance between effective hydrolysis for CNC production and minimal cellulose degradation. To definitively identify the optimal conditions, these samples were subsequently characterized using techniques like FTIR (Fourier-Transform Infrared Spectroscopy), AFM (Atomic Force Microscopy), and XRD (X-ray Diffraction). These characterization methods can provide an overall structure of the obtained CNCs, enabling the selection of the CNC sample with the most desirable characteristics for downstream applications.

3.4. Fourier transform infrared spectroscopy (FTIR)

FTIR analysis was employed to validate the chemical composition of the lignocellulosic materials, focusing on the identification of key organic functional groups. Fig. 4 reveals noticeable alterations in the peak intensities between the spectra of the untreated fiber (PALF), bleached cellulose, and CNF. Notably, a broad band persists across all spectra in the range of 3300–3400 cm^{-1}, which can be attributed to the O—H stretching vibrations of abundant hydroxyl groups present throughout the cellulose structure. The spectrum for untreated fiber exhibits bands at 2920 cm^{-1} and 2855 cm^{-1}, attributed primarily to the asymmetric and symmetric stretching modes of -CH_2 groups, respectively. In contrast, bleached cellulose spectrum displays a well-defined peak at 2895 cm^{-1} assigned to -CH stretching vibrations. This difference arises because a cellulose polymer chain harbors numerous distinct -CH bonds, each existing within a unique molecular environment. Consequently, with the removal of lignin and hemicellulose during the bleaching treatment, the -CH bonds respond differently [43]. Furthermore, the significant reduction in peak intensities observed at 1735 cm^{-1} and 1248 cm^{-1} provides compelling evidence for the diminished presence of lignin and hemicellulose after the treatments. The 1735 cm^{-1} peak corresponds to the stretching of a waxy C═O carboxylic group commonly found in hemicellulose, while the 1110 cm^{-1} peak can be attributed to the presence of C–O–C linkages characteristic of aryl-alkyl-ether bonds within lignin [44]. The untreated fiber spectrum also reveals a prominent band at 1520 cm^{-1}, indicative of C═C bond stretching within aromatic rings. This observation aligns with the presence of lignin, which possesses numerous such groups in its structure. Notably, this band exhibits a significant decrease in intensity within the spectra of bleached cellulose and CNF, further supporting the successful removal of lignin [45]. The presence of a peak at 895 cm^{-1} across all spectra characterizes the β-glycosidic linkages connecting glucose units in cellulose. This band corresponds to the glycosidic C_1-H deformation with contributions from ring vibration and OH bending. The observed increase in the intensity of this peak for bleached cellulose and CNF aligns with the enrichment of cellulosic components following the treatments [46]. These observations suggest that the implemented bleaching treatment effectively reduced the lignin content and conversely enriched the cellulose content.

Table 4
Yield of CNCs extracted from PALF under different acid hydrolysis conditions.

Sample	Yield (%)
CNC1	60.63
CNC2	36.80
CNC3	54.88
CNC4	2.47
CNC5	0.81
CNC6	0.67
CNC7	0.46

The efficacy of the acid hydrolysis treatments for CNC production was evaluated as presented in Fig. 5 By examining the FT-IR spectra of samples CNC1 to CNC7, alongside a mechanically produced CNF reference, valuable insights were obtained. Notably, a distinct peak at approximately 900 cm^{-1} was observed only in the spectra of CNC1 to CNC4. This band corresponds to the glycosidic linkage deformation of the C1—H bond, with contributions from both ring vibration and OH bending. This peak is characteristic of the β-glycosidic linkages connecting glucose units in the cellulose structure. Conversely, the absence of this peak in the spectra of CNC5 to CNC7 signifies degradation of the cellulose during the respective hydrolysis processes. This observation suggests that the hydrolysis conditions employed for CNC5 to CNC7 resulted in excessive cleavage of the glycosidic bonds, leading to the disintegration of the cellulose structure. While 64 wt% of sulfuric acid concentration is a commonly used condition for extracting CNC from various fiber sources, including pineapple leaves [17], this specific concentration did not yield satisfactory results for the pineapple leaf fiber of this study. Consequently, these three samples were excluded from further analyses due to their compromised structural integrity.

The appearance of a new absorption band at 800 cm^{-1} in the FTIR spectra of all CNC samples, with prominence in CNC5 to CNC7, is a notable finding. This band is attributed to the symmetrical stretching of the C-O-S bond, indicating the presence of sulfate groups within the CNC structure [47]. The increased intensity of this band in CNC5 to CNC7, which were previously identified as having undergone significant degradation during acid hydrolysis, suggests a direct correlation between the extent of cellulose degradation and the incorporation of sulfate groups. This observation suggests that harsher hydrolysis conditions employed for CNC5 to CNC7 resulted in the preferential cleavage of glycosidic bonds, leading to the formation of reactive sites that readily react with sulfuric acid, resulting in the introduction of sulfate groups onto the cellulose backbone.

In the case of CNC1 and CNC2 samples, they were only ones that showed defined peaks in the 1163 cm^{-1} and 1111 cm^{-1} bands, which refer to the symmetric and asymmetric stretching of the S═O bonds, respectively [48]. This observation suggests that the milder hydrolysis conditions employed for these samples maintained a more intact cellulose structure, allowing for the detection of the characteristic S═O stretching vibrations. The absence of these defined peaks in CNC3 to CNC7 may be attributed to the more extensive degradation of the cellulose structure, obscuring the detection of the S═O stretching bands.

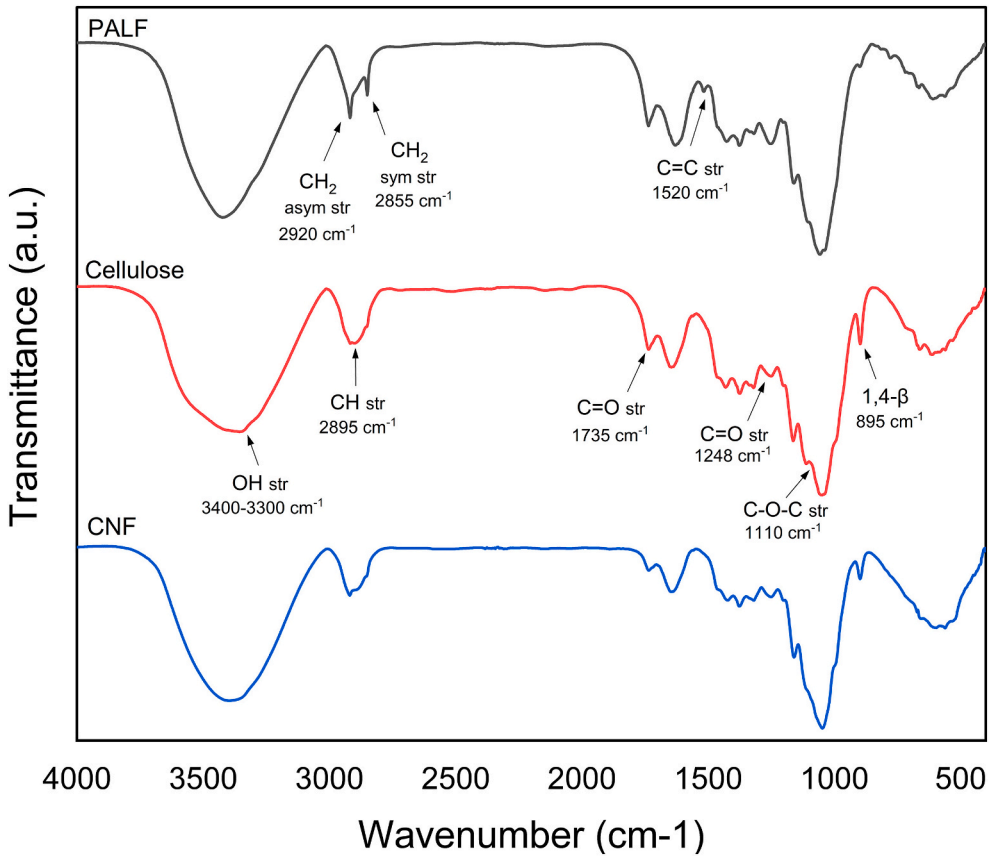

Fig. 4. FT-IR spectrum of PALF, cellulose and CNF fibers.

It is noteworthy that all FT-IR spectra exhibited a prominent broad band in the range of 3400–3450 cm^{-1}, attributed to the O—H stretching vibrations of hydroxyl groups. Additionally, a band observed in the range 2842–2919 cm^{-1} corresponds to the C—H stretching vibrations of aliphatic moieties within the polysaccharide backbone. Furthermore, a characteristic peak at 1043 cm^{-1} was identified, which can be assigned to the C-O-C pyranose ring skeletal vibrations present in the cellulose structure. These observations collectively confirm the presence of the key functional groups associated with cellulose in the successfully prepared CNC samples (CNC1 to CNC4).

3.5. X-ray diffraction (XRD)

X-ray Diffraction analysis was performed to investigate the crystalline structure of the untreated fiber, bleached cellulose, and CNF, as illustrated in Fig. 6. The diffractogram of PALF fiber revealed a pattern characteristic of Iβ cellulose, verified by the presence of peaks of Bragg's angle (2θ) at around 15° (plane 1–10), 16.5° (plane 110), 22.5° (plane 200) and 34.8° (plane 004) [41,49,50], with a crystallinity degree of 49.1 %, as detailed in Table 5. In contrast, the bleached cellulose exhibited a similar Iβ cellulose pattern, but with significantly enhanced crystallinity compared to PALF fiber, with crystallinity index of 64.7 %. This observation indicates that the alkali and bleaching process likely removed amorphous non-cellulosic components, leading to a more crystalline cellulose fraction. A similar crystallinity index was reported for PALF and the extracted cellulose in a previous study [41]. The CNF diffractogram displayed several broad bumps, suggesting a material with very low crystallinity. The application of the Segal method, a common technique for quantifying crystallinity from XRD data, was not feasible due to the lack of the valley at 18–19°. Interestingly, minor peaks corresponding to SiO_2 (quartz form) were also identified in the CNF spectrum at 26.6° [49]. This presence can be attributed to the potential release of minute particles from the ceramic grinding media used during the mechanical processing of cellulose into CNF.

Fig. 7 presents the XRD patterns of CNCs obtained under various conditions. Notably, CNC1, CNC2, and CNC3 all exhibited diffractograms characteristic of the Iβ Cellulose phase. This indicates that the employed hydrolysis conditions successfully preserved the crystalline structure of cellulose during CNC production. Conversely, when the acid concentration was increased from 55 % to 64 % (CNC4), the characteristics of cellulose Iβ were lost, the diffractogram displayed one prominent broad peak from 15° to 30°, a signature of amorphous materials, likely originating from fragmented cellulose. Additionally, three relatively sharper peaks were observed at 21.6°, 24.0° and 26.8°, potentially indicative of inorganic contaminants introduced during processing. CNC1, CNC2, and CNC3 demonstrated crystallinity values ranging from 79 % to 80 %. These results suggest that the chosen hydrolysis conditions effectively maintained a high degree of crystallinity within the resulting CNCs. However, CNC4, as corroborated by AFM analysis, displayed a significantly lower crystallinity index and lacked well-defined diffraction peaks, rendering the Segal method inapplicable for its crystallinity determination since there was no valley at 18–19°. This implies that the high acid concentration employed for CNC4 might have resulted in excessive fragmentation and disruption of the crystalline cellulose structure.

3.6. Atomic force microscopy (AFM)

AFM analysis was employed to investigate the surface morphology and dimensions of CNF and CNC samples. The results, as summarized in Table 6 and visually depicted in Fig. 8, reveal distinct morphological characteristics associated with the varying processing conditions. For CNF, the extended processing time of 196 h successfully produced nanofibers with an average length of approximately 256 nm. However,

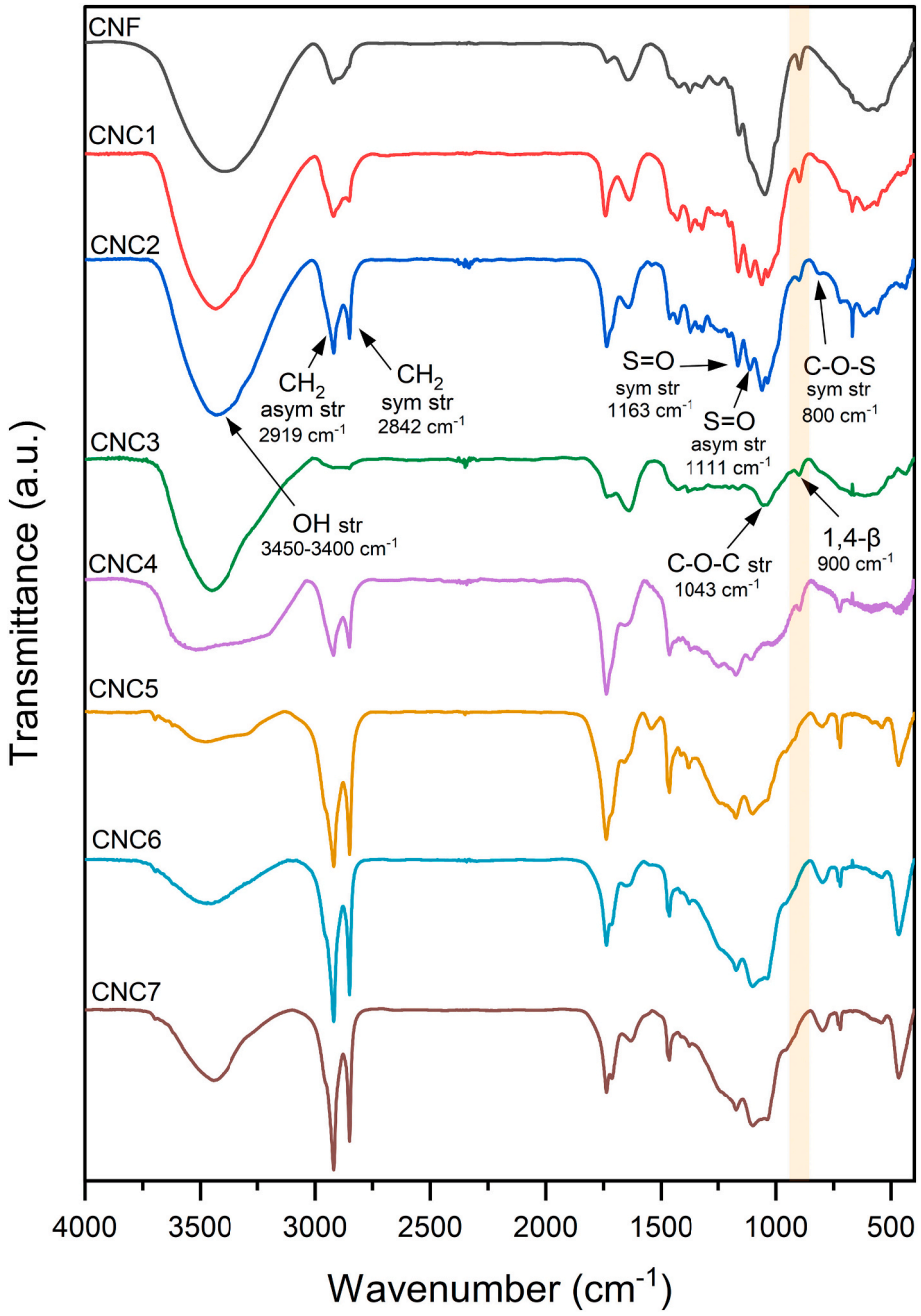

Fig. 5. FT-IR spectrum of CNF and CNCs obtained by different methods.

the fibers exhibited insufficient fibrillation and extensive fragmentation, likely caused by the prolonged mechanical processing time employed during ball milling. In contrast, CNC samples exhibited a more diverse range of morphologies. CNC1 and CNC3, prepared with lower sample solution-ratios of 20 to 50 mg/mL, displayed extensive networks of elongated fibers with a distinct crystalline-like shape. This suggests that the milder conditions employed during their preparation favored the formation of more intact and ordered nanocellulose structures. CNC2, prepared with a higher sample-solution concentration of 125 mg/mL, lacked this crystalline morphology but still possessed some fiber network structure. The increased concentration might have led to greater fiber-fiber interactions, hindering the development of a crystalline structure. Interestingly, CNC1 and CNC2 exhibited similar fiber lengths, averaging around 650–700 nm, and high compared to fragmented CNF. However, CNC3 presented significantly longer fibers with an average length of 1042 nm. This suggests that the extended hydrolysis time used in CNC3 preparation allowed for the formation of longer fibers. CNC4, on the other hand, displayed a markedly different morphology, characterized by highly fragmented and coarse fibers. Despite having the highest average length (1105 nm), these fibers lacked substantial continuity and appeared highly disrupted. Only the larger fibers could be measure, while the irregularly shaped ones could not. This is likely due to the higher acid concentration employed in CNC4 preparation, which may have resulted in excessive degradation of the cellulose structure. These results were confirmed by polarized optical microscopy (POM) and transmission electron microscopy (TEM) analyses, represented by Figs. S2 and S3, and Table S1.

Cellulose nanocrystals are typically defined as rod-shaped particles with a high aspect ratio (length-to-width ratio) [51,52]. Therefore, samples CNC1 and CNC2 have a relatively high length for this

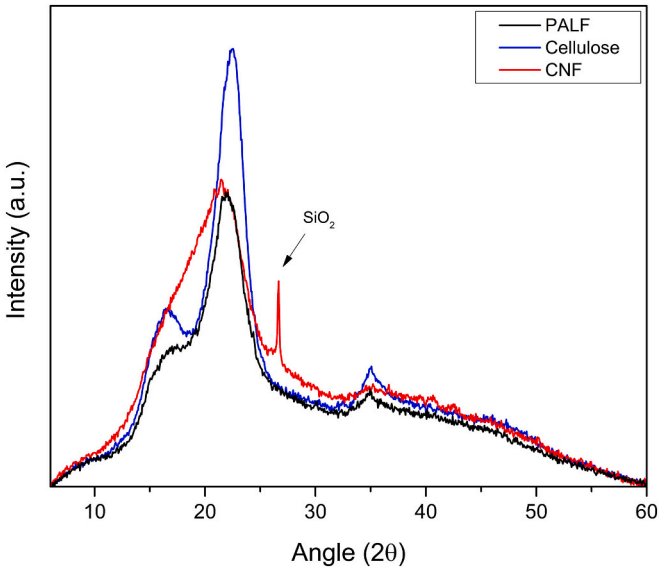

Fig. 6. XRD spectrum of PALF, cellulose, and CNF fibers.

Table 5
Crystallinity index for PALF, cellulose, CNF and CNCs fibers.

Sample	CrI (%)
PALF	49.1
Cellulose	64.7
CNF	–
CNC1	79.0
CNC2	79.2
CNC3	80.5
CNC4	–

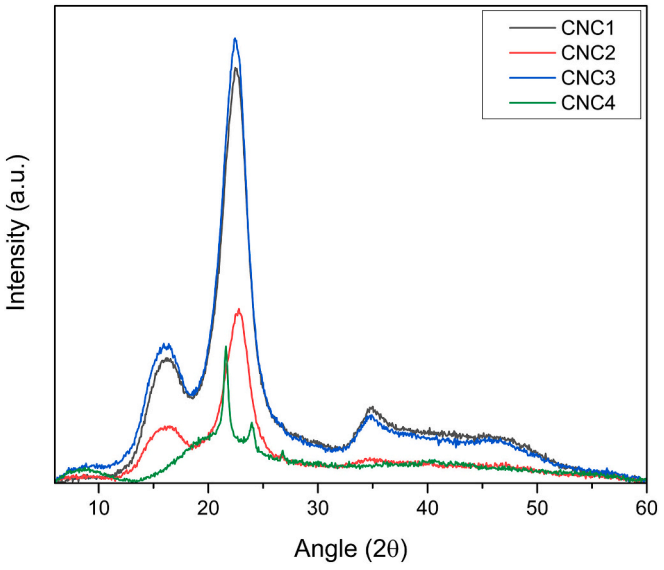

Fig. 7. XRD spectrum of CNCs obtained by different methods.

classification, although some researchers still consider as CNC if this larger particle still exhibits the characteristic properties of CNC, such as high crystallinity and a rod-like shape [17]. However, CNC3 and CNC4 exceed 1 μm in length and might not be classified as a CNC. Such particles would likely be considered microcrystalline cellulose (MCC) or cellulose microfibrils. Regarding CNF, they are typically long with an

Table 6
Count number and size of fibers analyzed by AFM.

Sample	Width (nm)	Count	Length (nm)	Count	Aspect ratio (l/w)
CNF	54 ± 15	60	256 ± 96	54	4.7 ± 2.2
CNC1	52 ± 9	61	700 ± 336	45	13.5 ± 6.2
CNC2	51 ± 12	54	647 ± 459	45	14.9 ± 13.7
CNC3	78 ± 21	44	1042 ± 390	21	14.1 ± 6.3
CNC4	85 ± 10	42	1105 ± 453	32	13.3 ± 6.1

aspect ratio exceeding 100 [51]. The lower aspect ratio observed in the CNF sample, with an average length of 256 nm, suggests that it may be more accurately classified just as cellulose nanoparticles (CNP) rather than nanofibrils of cellulose (CNF). The ball milling process appears to have resulted in the fragmentation of cellulose fibers into smaller particles, rather than the separation of individual fibrils. These particles, while similar in morphology to CNC, exhibit lower crystallinity compared to traditional CNC, as seen by XRD results, which are typically produced through acid hydrolysis.

Based on these combined AFM and XRD findings, the methods employed for obtaining CNC1 and CNC2 appear to yield more structurally desirable results. These samples exhibited a good balance between fiber length and crystallinity, suggesting their potential suitability for various downstream applications. Cellulose nanocrystals with good length have diverse applications due to their mechanical strength, nanoscale dimensions, and surface functionality. They reinforce composites, enhancing thin polymer films, though dispersion challenges remain. CNCs strengthen paper and cardboard while improving barrier properties in packaging and coatings. They enhance adhesives and support high-quality printing and 3D printing. Additionally, they also have biomedical applications in drug delivery, tissue engineering, and antimicrobial materials. These varied uses highlight CNCs' potential for innovation across industries [17]. Conversely, the extended processing time used for CNF resulted in excessive fragmentation and reduced crystallinity, probably limiting its performance in certain applications. However, it is still suitable to be incorporated into bio-based films for applications in food packaging, offering biodegradability and enhanced barrier properties [53]. Similarly, the method used for CNC4 yielded highly fragmented and poorly crystalline material, further diminishing its potential applications.

3.7. Thermogravimetric analysis (TGA)

The TGA results presented in Fig. 9 and Table 7 reveal significant differences in the thermal decomposition behavior of PALF, cellulose, CNF, and CNC samples obtained under various conditions. TGA showed lower decomposition onset temperature at 187 °C for PALF compared to bleached cellulose (249 °C), linked to hemicellulose degradation and cellulose glycosidic bond cleavage [49]. Furthermore, the lower decomposition temperature and higher residual mass at 600 °C for PALF is attributed to the presence of hemicellulose, lignin, and impurities that for cellulose is removed during bleaching [49]. A clear trend emerges, with cellulose exhibiting the highest decomposition temperature, followed by CNF, and then CNCs. For CNF, the ball milling process likely induces a decrease in molecular weight through mechanical shearing force of the cellulose chains. This reduction in chain length weakens the intermolecular forces within the cellulose structure, making it more susceptible to thermal degradation at lower temperatures compared to the cellulose. Similarly, the production of CNCs via acid hydrolysis also results in a rapid decrease in molecular weight. However, an additional factor contributes to the even lower decomposition temperatures observed for CNCs. The acid hydrolysis process typically involves the introduction of sulfate groups (SO_4^{2-}) into the amorphous regions of cellulose. These sulfated amorphous regions create a more accessible and less thermally stable environment within the CNC structure, facilitating the decomposition process at lower temperatures compared to

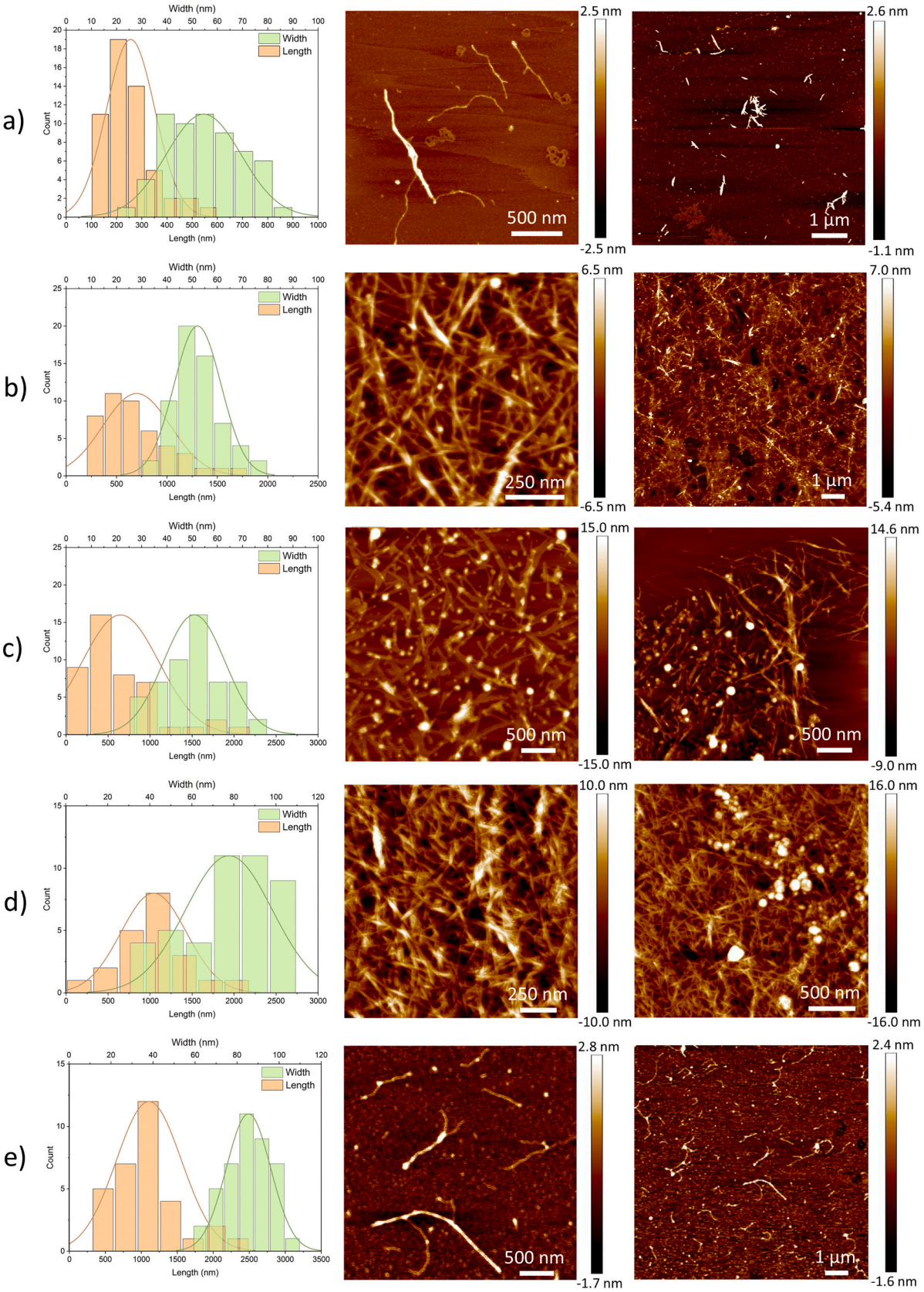

Fig. 8. AFM images and particle size distribution histogram of: (a) CNF; (b) CNC1; (c) CNC2; (d) CNC3; (e) CNC4.

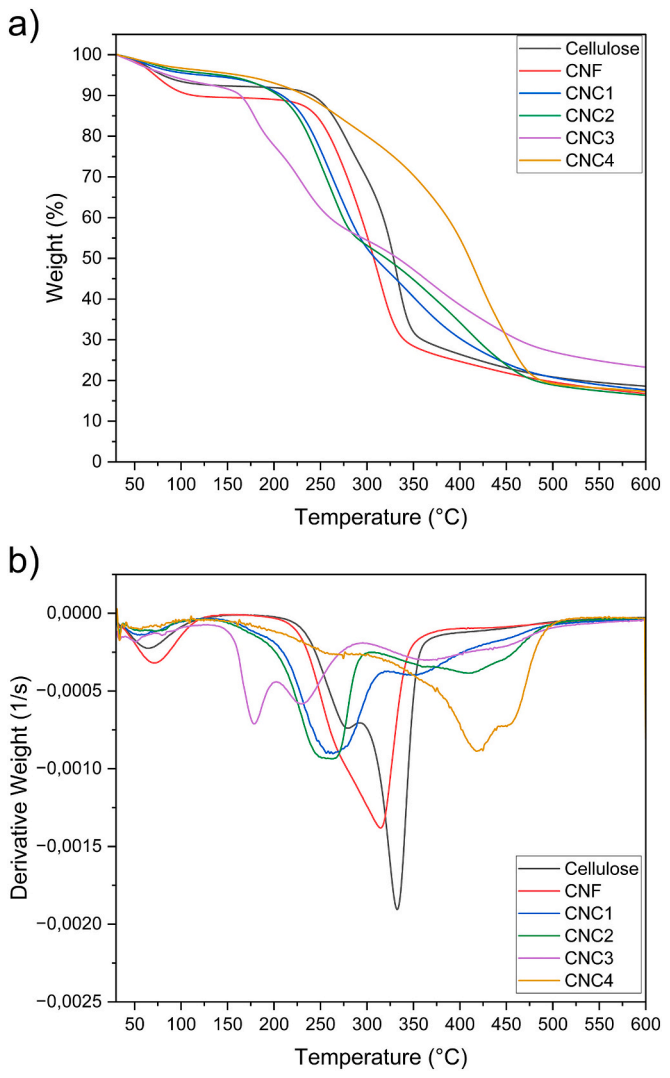

Fig. 9. (a) TGA and (b) DTG curves of cellulose, CNF and CNCs obtained under different conditions.

Table 7
Thermogravimetric analysis data for cellulose, CNF and CNCs obtained under different conditions.

Sample	T_{onset} (°C)	$T_{5\%}$ (°C)	$T_{50\%}$ (°C)	$T_{DTG\ max}$ (°C)	$R_{600°C}$ (%)
PALF	186.6	69.5	318.3	202.6 / 311.1	26.5
Cellulose	248.9	80.2	328.7	278.5 / 332.5	18.5
CNF	245.5	71.8	307.3	314.7	16.7
CNC1	216.4	123.5	309.0	263.4 / 347.3	17.4
CNC2	214.3	142.7	320.7	262.1 / 411.8	16.1
CNC3	164.6	86.2	333.3	178.5 / 229.4	23.1
CNC4	215.1	162.0	410.3	417.9 / 450.5	16.8

both cellulose and CNF [54].

The thermograms for all samples exhibit an initial weight loss step around 100 °C, likely corresponding to the evaporation of moisture content present within the samples. Subsequently, CNC1 and CNC2, obtained using similar hydrolysis conditions (55 % H_2SO_4, 45 °C, 30 min) with varying sample-to-solution ratios (20 mg/mL and 125 mg/mL respectively), display a similar decrease in decomposition temperature compared to cellulose. Their on-set decomposition temperatures are approximately 32 °C lower than that of cellulose. This suggests that the hydrolysis conditions employed for CNC1 and CNC2 were sufficient to achieve a reduction in molecular weight and introduce sulfate groups, leading to a similar decrease in thermal stability for both CNCs [55,56].

However, CNC3, obtained with a longer hydrolysis time (60 min) but the same acid concentration and temperature, presents a markedly distinct behavior. Its on-set decomposition temperature is significantly lower (164.6 °C) compared to other CNCs. This observation, coupled with its high residual mass (23 %), suggests that the extended hydrolysis time for CNC3 potentially resulted from the catalytic effect of the sulfate groups of CNCs with a larger non-volatile residue remaining after decomposition [56,57]. Two stages of decomposition can also be observed at 178.5 °C and 229.4 °C, consistent with findings reported by other authors [58–60]. The low-temperature phase is attributed to the degradation of the more accessible regions (amorphous regions), which are more sulfated and easier to break down. The second, higher-temperature phase corresponds to the breakdown of the crystalline fraction, which remained intact and unaffected by sulfuric acid. Finally, CNC4, obtained using a higher acid concentration (64 % H_2SO_4) but a shorter hydrolysis time (15 min), exhibits a unique decomposition pattern. While its on-set decomposition temperature (215.1 °C) aligns more closely with CNC1 and CNC2, its weight loss profile displays a slower and more gradual decrease in mass compared to the other samples. This behavior occurred since increasing quantities of sulfate groups can lead to a broader degradation temperature range, which can compromise the cellulose's crystalline structure, as observed by others [56,61]. This interpretation is further supported by XRD analysis, which showed the loss of the Iβ cellulose structure in CNC4. These findings collectively indicate that the aggressive acid hydrolysis conditions (high acid concentration), resulting in an altered material with properties distinct from typical CNC.

4. Conclusion

This study investigated acid hydrolysis conditions for extracting cellulose nanocrystals (CNC) and cellulose nanofibrils (CNF) from pineapple leaf fibers (PALF), aiming to optimize yield and quality. The high holocellulose (64.67 %) and α-cellulose (78.14 %) content of PALF confirmed its suitability as a source of cellulosic material, while the presence of lignin (18.95 %) emphasized the need for effective lignin removal to enhance CNC accessibility. The findings revealed that milder hydrolysis conditions (lower temperature of 45 °C, lower acid concentration of 55 %, and sample-to-solution ratios of 20–50 mg/mL) were optimal for preserving cellulose structure, achieving high crystallinity, and minimizing thermal degradation.

CNC samples CNC1 and CNC2 demonstrated the most promising characteristics, including preservation of crystallinity and appropriate fiber dimensions. In contrast, the study also identified some limitations. Higher acid concentration (64 %) and higher temperature (55 °C) led to the introduction of additional sulfate groups, accelerating the thermal degradation of CNCs and compromising their stability. Moreover, increased viscosity from higher sample-to-solution ratios hindered hydrolysis, resulting in CNCs with inconsistent dimensions. For CNF production, mechanical processing for longer hours disrupted the crystalline structures, leading to nanoparticle aggregates rather than well-defined nanofibers, which may affect their desired properties. To optimize the fibrillation of CNF, processing times shorter than 196 h should be further investigated.

Despite these challenges, PALF proves to be a promising feedstock for nanocellulose production. Its high cellulose content and favorable chemical composition make it a suitable candidate for CNC extraction. By optimizing processing conditions, PALF-derived CNC can be tailored for various applications, including biocomposites, drug delivery, and tissue engineering. Further research and development are necessary to fully realize the potential of PALF as a sustainable source for high-performance nanocellulose materials.

CRediT authorship contribution statement

Fernanda Andrade Tigre da Costa: Writing – original draft, Visualization, Methodology, Investigation, Formal analysis, Data curation, Conceptualization. **Alain Dufresne:** Writing – review & editing, Supervision. **Tao Song:** Writing – review & editing. **Duclerc Fernandes Parra:** Writing – review & editing, Supervision.

Declaration of competing interest

The authors declare that they have no known competing financial interests or personal relationships that could have appeared to influence the work reported in this paper.

Acknowledgements

To the support of CNPq and IPEN/CNEN. LGP2, part of the LabEx Tec 21 (Investissements d'Avenir - grant agreement n°ANR-11-LABX-0030) and of the PolyNat Carnot Institut (Investissements d'Avenir - grant agreement n°ANR-11-CARN-030-01). Financial support from the Project to Attract Foreign Experts by MOST (G2023163006L).

Appendix A. Supplementary data

Supplementary data to this article can be found online at https://doi.org/10.1016/j.ijbiomac.2025.141755.

References

[1] D. Klemm, F. Kramer, S. Moritz, et al., Nanocelluloses: a new family of nature-based materials, Angew. Chem. Int. Ed. 50 (2011) 5438–5466, https://doi.org/10.1002/anie.201001273.
[2] R.F. Grossman, D. Nwabunma, Biopolymer Nanocomposites: Processing, Properties, and Applications, John Wiley & Sons, 2013.
[3] Y. Habibi, L.A. Lucia, O.J. Rojas, Cellulose nanocrystals: chemistry, self-assembly, and applications, Chem. Rev. 110 (2010) 3479–3500, https://doi.org/10.1021/cr900339w.
[4] A. Abbasi Moud, A. Abbasi Moud, Flow and assembly of cellulose nanocrystals (CNC): a bottom-up perspective - a review, Int. J. Biol. Macromol. 232 (2023) 123391, https://doi.org/10.1016/j.ijbiomac.2023.123391.
[5] T. Yi, H. Zhao, Q. Mo, et al., From cellulose to cellulose Nanofibrils—a comprehensive review of the preparation and modification of cellulose Nanofibrils, Materials 13 (2020) 5062, https://doi.org/10.3390/ma13225062.
[6] A. Blanco, M.C. Monte, C. Campano, et al., Nanocellulose for Industrial Use, in: Handbook of Nanomaterials for Industrial Applications, Elsevier, 2018, pp. 74–126.
[7] Dutta S, Devi RR (2020) Cellulose nanofibers from agro-wastes of Northeast India for nanocomposite and bioenergy applications. pp 149–172.
[8] Jaramillo-Quiceno N, Vélez R. JM, Cadena Ch. EM, et al (2018) Improvement of mechanical properties of pineapple leaf fibers by mercerization process. Fibers Polymers 19:2604–2611. doi:https://doi.org/10.1007/s12221-018-8522-3.
[9] FAOSTAT (2023) Crops and livestock products. In: https://www.fao.org/faostat/en/#data/QCL.
[10] F.N.M. Padzil, Z.M.A. Ainun, N. Abu Kassim, et al., Chemical, Physical and Biological Treatments of Pineapple Leaf Fibres, in: Green Energy and Technology, Springer Science and Business Media Deutschland GmbH, 2020, pp. 73–90.
[11] A.F. Aili Hamzah, M.H. Hamzah, H. Che Man, et al., Recent updates on the conversion of pineapple waste (Ananas comosus) to value-added products, Future Perspectives and Challenges, Agronomy 11 (2021) 2221, https://doi.org/10.3390/agronomy11112221.
[12] A. Chen, Y.J. Guan, M. Bustamante, et al., Production of renewable fuel and value-added bioproducts using pineapple leaves in Costa Rica, Biomass Bioenergy 141 (2020) 105675, https://doi.org/10.1016/j.biombioe.2020.105675.
[13] M. Zubair, N.D. Mu'azu, M. Nasir, et al., Cellulose nanocrystals from office paper waste for green mortar: process optimization modeling, characterization, and mechanical properties, Arab. J. Sci. Eng. 47 (2022) 5377–5393, https://doi.org/10.1007/s13369-022-06609-8.
[14] W. Liu, H. Du, H. Liu, et al., Highly efficient and sustainable preparation of carboxylic and thermostable cellulose nanocrystals via $FeCl_3$ -catalyzed innocuous citric acid hydrolysis, ACS Sustain. Chem. Eng. 8 (2020) 16691–16700, https://doi.org/10.1021/acssuschemeng.0c06561.
[15] L. Chen, Q. Wang, K. Hirth, et al., Tailoring the yield and characteristics of wood cellulose nanocrystals (CNC) using concentrated acid hydrolysis, Cellulose 22 (2015) 1753–1762, https://doi.org/10.1007/s10570-015-0615-1.
[16] Q.Q. Wang, J.Y. Zhu, R.S. Reiner, et al., Approaching zero cellulose loss in cellulose nanocrystal (CNC) production: recovery and characterization of cellulosic solid residues (CSR) and CNC, Cellulose 19 (2012) 2033–2047, https://doi.org/10.1007/s10570-012-9765-6.
[17] A. Dufresne, Nanocellulose: From Nature to High Performance Tailored Materials, 2nd ed, Walter de Gruyter GmbH & Co KG, 2017.
[18] B. Anwar, B. Bundjali, I.M. Arcana, Isolation of cellulose nanocrystals from bacterial cellulose produced from pineapple Peel waste juice as culture medium, Proc. Chem 16 (2015) 279–284, https://doi.org/10.1016/j.proche.2015.12.051.
[19] K.S. Prado, M.A.S. Spinacé, Isolation and characterization of cellulose nanocrystals from pineapple crown waste and their potential uses, Int. J. Biol. Macromol. 122 (2019) 410–416, https://doi.org/10.1016/j.ijbiomac.2018.10.187.
[20] S.L. Leong, S.I.X. Tiong, S.P. Siva, et al., Morphological control of cellulose nanocrystals via sulfuric acid hydrolysis based on sustainability considerations: an overview of the governing factors and potential challenges, J. Environ. Chem. Eng. 10 (2022) 108145, https://doi.org/10.1016/j.jece.2022.108145.
[21] Y. Tang, H. Yang, S. Vignolini, Recent Progress in production methods for cellulose nanocrystals: leading to more sustainable processes, Adv. Sustain. Syst. 6 (2022), https://doi.org/10.1002/adsu.202100100.
[22] L. Wang, K. Li, K. Copenhaver, et al., Review on nonconventional fibrillation methods of producing cellulose Nanofibrils and their applications, Biomacromolecules 22 (2021) 4037–4059, https://doi.org/10.1021/acs.biomac.1c00640.
[23] P. Huang, C. Wang, Y. Huang, M. Wu, Structure and Properties of Cellulose Nanofibrils, in: Nanocellulose, Wiley, 2019, pp. 53–80.
[24] M. Ilangovan, V. Guna, B. Prajwal, et al., Extraction and characterisation of natural cellulose fibers from Kigelia africana, Carbohydr. Polym. 236 (2020) 115996, https://doi.org/10.1016/j.carbpol.2020.115996.
[25] T.I. Shaheen, H.E. Emam, Sono-chemical synthesis of cellulose nanocrystals from wood sawdust using acid hydrolysis, Int. J. Biol. Macromol. 107 (2018) 1599–1606, https://doi.org/10.1016/j.ijbiomac.2017.10.028.
[26] Technical Association of the Pulp and Paper Industry (2007) Solvent extractives of wood and pulp (Proposed revision of T 204 cm-97). TAPPI test methods 7–10.
[27] Technical Association of the Pulp and Paper Industry (2007) Preparation of wood for chemical analysis. TAPPI test methods 1–4.
[28] Technical Association of the Pulp and Paper Industry (2007) Ash in wood, pulp, paper and paperboard: combustion at 525 C. TAPPI test methods 1–7.
[29] Technical Association of the Pulp and Paper Industry (2006) Acid-insoluble lignin in wood and pulp. TAPPI testz methods 14.
[30] Wise Le, M. Murphy, A.A. D'Addieco, Chlorite Holocellulose, its Fractionnation and Bearing on Summative Wood Analysis and on Studies on the Hemicelluloses, Vance, New York, 1946.
[31] Technical Association of the Pulp and Paper Industry (1999) Alpha-, beta- and gamma-cellulose in pulp. TAPPI test methods 5–9.
[32] S. Nam, A.D. French, B.D. Condon, M. Concha, Segal crystallinity index revisited by the simulation of X-ray diffraction patterns of cotton cellulose Iβ and cellulose II, Carbohydr. Polym. 135 (2016) 1–9, https://doi.org/10.1016/j.carbpol.2015.08.035.
[33] L. Marynowski, M. Goryl, M. Lempart-Drozd, et al., Differences in hemicellulose composition and pectin detection in Eocene and Miocene xylites, Chem. Geol. 624 (2023) 121416, https://doi.org/10.1016/j.chemgeo.2023.121416.
[34] M. Jonoobi, R. Oladi, Y. Davoudpour, et al., Different preparation methods and properties of nanostructured cellulose from various natural resources and residues: a review, Cellulose 22 (2015) 935–969, https://doi.org/10.1007/s10570-015-0551-0.
[35] L. Hu, X. Fang, M. Du, et al., Hemicellulose-based polymers processing and application, Am. J. Plant Sci. 11 (2020) 2066–2079, https://doi.org/10.4236/ajps.2020.1112146.
[36] A. Karimah, M.R. Ridho, S.S. Munawar, et al., A review on natural fibers for development of eco-friendly bio-composite: characteristics, and utilizations, J. Mater. Res. Technol. 13 (2021) 2442–2458, https://doi.org/10.1016/j.jmrt.2021.06.014.
[37] E. Triwulandari, M. Ghozali, D. Sondari, et al., Effect of lignin on mechanical, biodegradability, morphology, and thermal properties of polypropylene/polylactic acid/lignin biocomposite, Plast., Rubber Compos. 48 (2019) 82–92, https://doi.org/10.1080/14658011.2018.1562746.
[38] R.N. Wijesena, N.D. Tissera, V.W.S.G. Rathnayaka, et al., Colloidal stability of chitin nanofibers in aqueous systems: Effect of pH, ionic strength, temperature & concentration, Carbohydr. Polym. 235 (2020) 116024, https://doi.org/10.1016/j.carbpol.2020.116024.
[39] S.M. Mohomane, S.V. Motloung, L.F. Koao, Motaung Te, Effects of acid hydrolysis on the extraction of cellulose nanocrystals (cncs): a review, Cellul. Chem. Technol. 56 (2022) 691–703, https://doi.org/10.35812/CelluloseChemTechnol.2022.56.61.
[40] J.L. Sanchez-Salvador, H. Xu, A. Balea, et al., Nanocellulose from a colloidal material perspective, Front. Mater. 10 (2023), https://doi.org/10.3389/fmats.2023.1231404.
[41] Santos RM dos, Flauzino Neto WP, Silvério HA, et al (2013) Cellulose nanocrystals from pineapple leaf, a new approach for the reuse of this agro-waste. Ind. Crop. Prod. 50:707–714. doi:https://doi.org/10.1016/j.indcrop.2013.08.049.
[42] Q. Wang, X. Zhao, J.Y. Zhu, Kinetics of strong acid hydrolysis of a bleached Kraft pulp for producing cellulose nanocrystals (CNCs), Ind. Eng. Chem. Res. 53 (2014) 11007–11014, https://doi.org/10.1021/ie501672m.
[43] S. Kokot, B. Czarnik-Matusewicz, Y. Ozaki, Two-dimensional correlation spectroscopy and principal component analysis studies of temperature-dependent IR spectra of cotton–cellulose, Biopolymers 67 (2002) 456–469, https://doi.org/10.1002/bip.10163.

[44] U. Qasim, Z. Ali, M.S. Nazir, et al., Isolation of cellulose from wheat straw using alkaline hydrogen peroxide and acidified sodium chlorite treatments: comparison of yield and properties, Adv. Polym. Technol. 2020 (2020) 1–7, https://doi.org/10.1155/2020/9765950.
[45] E.M.S. Cordeiro, Y.L. Nunes, A.L.A. Mattos, et al., Polymer biocomposites and Nanobiocomposites obtained from mango seeds, Macromol. Symp. 344 (2014) 39–54, https://doi.org/10.1002/masy.201300217.
[46] F. Kallel, F. Bettaieb, R. Khiari, et al., Isolation and structural characterization of cellulose nanocrystals extracted from garlic straw residues, Ind. Crop. Prod. 87 (2016) 287–296, https://doi.org/10.1016/j.indcrop.2016.04.060.
[47] M. Börjesson, K. Sahlin, D. Bernin, G. Westman, Increased thermal stability of nanocellulose composites by functionalization of the sulfate groups on cellulose nanocrystals with azetidinium ions, J. Appl. Polym. Sci. 135 (2018), https://doi.org/10.1002/app.45963.
[48] B. Wang, R. Li, J. Zeng, et al., Preparation of cellulose nanocrystals via successive periodate and bisulfite oxidation and mechanical and hydrophilic properties of the films, Bioresources 16 (2021) 1713–1725, https://doi.org/10.15376/biores.16.1.1713-1725.
[49] M. Islam, A.S.K. Sinha, K. Prasad, Organosolv delignification of rice straw cellulose fiber for functional food packaging, Cellulose 31 (2024) 9191–9214, https://doi.org/10.1007/s10570-024-06125-y.
[50] I.M. Fareez, N.A. Ibrahim, W.M.H. Wan Yaacob, et al., Characteristics of cellulose extracted from Josapine pineapple leaf fibre after alkali treatment followed by extensive bleaching, Cellulose 25 (2018) 4407–4421, https://doi.org/10.1007/s10570-018-1878-0.
[51] B. Frka-Petesic, T.G. Parton, C. Honorato-Rios, et al., Structural color from cellulose nanocrystals or chitin nanocrystals: self-assembly, optics, and applications, Chem. Rev. 123 (2023) 12595–12756, https://doi.org/10.1021/acs.chemrev.2c00836.
[52] R. Wang, H. He, J. Tian, et al., Solvent-dependent dynamics of cellulose nanocrystals in process-relevant flow fields, Langmuir 40 (2024) 13319–13329, https://doi.org/10.1021/acs.langmuir.4c01846.
[53] U. Milbreta, L. Andze, I. Filipova, E. Dortins, Effect of nanofibrillated cellulose on alginate and chitosan film properties as potential barrier coatings for paper food packaging, Bioresources 19 (2024) 3375–3389, https://doi.org/10.15376/biores.19.2.3375-3389.
[54] D.-Y. Kim, B.-M. Lee, D.H. Koo, et al., Preparation of nanocellulose from a kenaf core using E-beam irradiation and acid hydrolysis, Cellulose 23 (2016) 3039–3049, https://doi.org/10.1007/s10570-016-1037-4.
[55] H. Kargarzadeh, I. Ahmad, I. Abdullah, et al., Effects of hydrolysis conditions on the morphology, crystallinity, and thermal stability of cellulose nanocrystals extracted from kenaf bast fibers, Cellulose 19 (2012) 855–866, https://doi.org/10.1007/s10570-012-9684-6.
[56] M. Roman, W.T. Winter, Effect of sulfate groups from sulfuric acid hydrolysis on the thermal degradation behavior of bacterial cellulose, Biomacromolecules 5 (2004) 1671–1677, https://doi.org/10.1021/bm034519+.
[57] Y. Park, M. You, J. Shin, et al., Thermal conductivity enhancement in electrospun poly(vinyl alcohol) and poly(vinyl alcohol)/cellulose nanocrystal composite nanofibers, Sci. Rep. 9 (2019) 3026, https://doi.org/10.1038/s41598-019-39825-8.
[58] H.A. Silvério, W.P. Flauzino Neto, N.O. Dantas, D. Pasquini, Extraction and characterization of cellulose nanocrystals from corncob for application as reinforcing agent in nanocomposites, Ind. Crop. Prod. 44 (2013) 427–436, https://doi.org/10.1016/j.indcrop.2012.10.014.
[59] A. Merlini, C. Claumann, A.W. Zibetti, et al., Kinetic study of the thermal decomposition of cellulose nanocrystals with different crystal structures and morphologies, Ind. Eng. Chem. Res. 59 (2020) 13428–13439, https://doi.org/10.1021/acs.iecr.0c01444.
[60] R. Li, J. Fei, Y. Cai, et al., Cellulose whiskers extracted from mulberry: a novel biomass production, Carbohydr. Polym. 76 (2009) 94–99, https://doi.org/10.1016/j.carbpol.2008.09.034.
[61] E. Mascheroni, R. Rampazzo, M.A. Ortenzi, et al., Comparison of cellulose nanocrystals obtained by sulfuric acid hydrolysis and ammonium persulfate, to be used as coating on flexible food-packaging materials, Cellulose 23 (2016) 779–793, https://doi.org/10.1007/s10570-015-0853-2.